VSC-based LVDC distribution network with DERs: equivalent circuits for leakage and ground fault currents evaluation

Simone Negri[a], Enrico Tironi[a], Gabrio Superti-Furga[a], Marco Carminati[b]

[a] Dipartimento di Elettronica, Informazione e Bioingegneria, Politecnico di Milano, piazza Leonardo da Vinci 32, 20133, Milano, Italy

[b] ABB S.p.a | SACE, Via Pescaria, 5, 24123 Bergamo (BG), Italy

E-mail addresses: simone.negri@polimi.it, enrico.tironi@polimi.it, gabrio.supertifurga@polimi.it, marco.carminati@it.abb.com.

***Abstract*— In this paper a new, general methodology for leakage and ground fault currents evaluation in grid-connected, low-voltage DC microgrids is introduced. Modified sequence equivalent circuits are considered, generalizing traditional AC power systems analysis. For three-phase systems, a modified Clarke transformation and, for two-wire systems, a modified modal transformation are introduced. These transformations, applied to a hybrid AC/DC system, allow building a modal equivalent circuit of the whole system, constituted by two coupled sub-circuits. The proposed equivalent circuits are intended as general time-domain models and are suitable for both steady-state and transient analysis. This approach highlights the whole system topology and allows evaluating the influence of active and passive components on leakage and ground fault currents. The proposed methodology is experimentally verified and, successively, applied to a hybrid AC/DC microgrid including DERs and storage devices.**

Keywords—DERs, LVDC distribution, Ground fault analysis, Leakage currents, DC system grounding, modal equivalent circuits.

1. INTRODUCTION

New scenarios are opening for electric power distribution systems. Environmental concerns are pushing towards massive diffusion of distributed generation provided by renewable energy sources, mainly wind and photovoltaic (PV). In particular, new directives from European Community [1] are directing Member States towards decarbonisation, drastically reducing the use of fossil fuels, improving the efficiency of the whole electrical system from generation to utilization and encouraging different forms of self-consumption. This trend is clearly reflected in literature, where many recent studies about PV modelling [2][3], performance analysis and degradation assessment [4]-[6] are recognized. Similarly, microgrid operation is widely discussed [7]-[12]. Another ongoing transformation in electrical world is the (re)introduction of DC distribution systems. The advantages of DC systems include increased power transmission capability, lower power losses, improved power quality and easier access for the many DC loads. Additionally, DC systems provide easier integration for renewable energy sources and storage devices [13].

From these considerations, it is reasonable to foresee quite a diffusion of DC microgrids. The latter are easily expandable and can be connected to the public three-phase AC distribution system by means of Voltage-Source Converters (VSCs). The presence of IGBT-based, AC/DC power converters interfacing the public AC system to a DC grid can cause power quality issues in the former [14]. Additionally, it can create non-negligible issues in case of faults affecting the DC grid and, possibly, even in normal operating condition, due to the circulation of common-mode leakage currents [15]-[20].

This paper is focused on leakage and ground fault currents evaluation in low voltage DC microgrids connected to the public AC distribution system. The evaluation of high-frequency ground currents generated by VSC switching is not completely covered in literature. When the AC system is grounded and the DC system is isolated, those ground currents are driven by the voltage oscillations of the DC poles with respect to ground and affect the capacitances to ground of DC lines, loads and the AC system grounding arrangement [15]-[20]. Even though the amplitude of high-frequency ground currents is usually small, they can be a significant source of disturbances for electronic devices. Additionally, high-frequency ground currents can interfere with Residual Current Devices (RCD) installed in the AC system, possibly causing unwanted trips.

Considering now ground fault currents evaluation, the analysis of VSC behaviour in presence of Pole-to-Ground Faults (PGFs) on the DC section as a function of the fault loop resistance highlights a gradual control loss in IGBTs for decreasing fault loop resistance values [21]. In particular, during each AC voltage period the converter exhibits a succession of time intervals of normal behaviour and time intervals in which the converter works as a diode rectifier. For low fault resistance values, with consequent high fault current and significant drop of the DC voltage, IGBTs pass to block-state permanently and the converter works as a diode rectifier. Consequently, the detailed study of the PGF behaviour generally requires the simulation of the whole systems by means of suitable software tools, which are not always available nor commonly used by professional operators. For these reasons, it is common to introduce some kind of simplification in fault current evaluation. Even if the evaluation of fault currents in presence

of PGF is widely covered in literature [13], [22]-[28], this topic requires further study regarding some grid configurations. Various Authors address the problem of PGF by splitting it in different stages. Immediately after a PGF affects a VCS-based, LVDC distribution network, the VSC IGBTs are blocked for self-protection, leaving free-wheeling diodes exposed to the fault current. The discharge transient of the filter capacitors causes fast current increasing in the free-wheeling diodes, which can possibly damage the diodes themselves. This is usually the most critical phase of the PGF transient. If diodes survive this stage, as the DC bus voltage drops well below the grid voltage, the diodes became forward biased and the VSC acts as an uncontrolled rectifier.

This approach is surely suitable for any configuration in which the fault loop impedance is low, but it does not cover all possible cases. The situation may be radically different in case of hybrid AC/DC power systems with an isolated DC section, connected to an MV/LV transformer, whose neutral point is connected to a grounding arrangement separated from the DC exposed conductive parts. In this case, the grid fault current contribution is large enough to affect fault calculation accuracy. Therefore, it should be taken into account to obtain more accurate results. In addition, the fault current values are limited and the converter feeds the fault, maintaining control over IGBTs switching.

In order to address these issues, in this paper a new, general methodology for leakage and ground fault currents evaluation in hybrid power systems is proposed. Such systems usually include three interconnected subsystems, namely: three-phase systems (three wires), two-wire systems (typically DC), and single-wire systems (usually ground reclosing paths or three-phase systems fourth wire). These systems are connected by means of suitable interfaces, which can be active elements (e.g. AC/DC power converters) or simple passive connections (e.g. grounded star connection). The proposed methodology is based on equivalent circuits representing the whole AC/DC hybrid system: in particular, modified sequence equivalent circuits are proposed, generalizing what is traditionally done in AC power systems, where the zero-sequence equivalent circuit is the most common tool for ground-fault analysis. For three-phase systems, a modified Clarke transformation is proposed, while for two-wire systems a modified Common-Mode (CM) / Differential Mode (DM) transformation is introduced. The present analysis and the resulting equivalent circuits are intended as a general, time-domain model, which is then applied both in frequency-domain and time-domain analysis. The proposed approach allows highlighting significant aspects of the whole system topology. Moreover, during design phase, it allows evaluating the influence of different (active and passive) components on leakage and ground fault currents.

To highlight the effectiveness of the proposed equivalent circuits, a grid-connected DC microgrid including DERs and storage devices is considered. Two scenarios are evaluated: in the first one the MV/LV transformer neutral point is grounded, while, in the second one the neutral point is isolated. In both scenarios the DC exposed conductive parts are grounded. The second scenario is possible whether the transformer is owned by the End User.

The paper is organized as follows. Section 2 presents the methodological approach used by the Authors to build a suitable equivalent circuit. In Section 3, the experimental tests performed to validate the proposed model are reported. In Section 4, the proposed methodological approach is applied to the two aforementioned case studies. Section 5 presents some considerations related to protection design requirements. Finally, the paper conclusions are drawn in Section 6.

2. Generalized Space-Vector and Zero-Sequence Circuits

In this Section the proposed transformations for three-phase (AC) and two-wire (DC) networks are introduced. These transformations, applied to hybrid AC/DC systems, allow building modal equivalent circuits of the whole system, which result in two coupled sub-circuits. The first one, named Generalized Space-Vector Equivalent Circuit (GSVEC), consists of space-vector and DM equivalent circuits. This sub-circuit manages the fundamental functions of the system and usually carries most power. The second sub-circuit, named Generalized Zero-Sequence Equivalent Circuit (GZSEC), consists of zero-sequence and CM equivalent circuits, and possibly 4th-wire and ground network. These two sub-circuits interact by means of static converters, unbalanced lines/impedances and asymmetrical faults, and these interactions allow transferring power from GSVEC to GZSEC.

Transformations proposed in the following represent innovative, modified forms of well-established transformations. The proposed modifications allow achieving simpler equivalent circuits, in which the different subsystems are directly connected to each other. On the contrary, traditional transformations include reporting coefficients, proposed for instance in [29], which require a more complex equivalent circuit representation. In the following, each transformation is exemplified for voltages, currents, impedances and connections (e.g. star connection). Additionally, the equivalent circuits of AC/DC and DC/DC converters are presented. These represent the building blocks of the complete equivalent circuits presented in later Sections.

2.1. Three-phase transformation

2.1.1. Voltages and currents

Three-phase voltages v_a, v_b, v_c and currents i_a, i_b, i_c are transformed by means of a modified Clarke transformation, resulting in space-vectors **v, i** and zero components v_0, i_0, namely:

$$\mathbf{v} = v_\alpha + jv_\beta = \sqrt{2/3}\left(v_a + \alpha v_b + \alpha^2 v_c\right), \quad \alpha = e^{j\frac{2}{3}\pi}$$
$$v_0 = \left(v_a + v_b + v_c\right)/3 \tag{1}$$

$$\mathbf{i} = i_\alpha + ji_\beta = \sqrt{2/3}\left(i_a + \alpha i_b + \alpha^2 i_c\right), \; i_0 = i_a + i_b + i_c \tag{2}$$

Note that the space vector components v_α, v_β and i_α, i_β, are identical to the traditional Clarke transformation [30]-[33]. On

the contrary, the zero components v_0, i_0 are defined differently, and voltage and current transformations differ from each other. In matrix form, (1) and (2) can be rewritten as

$$\begin{bmatrix} v_\alpha \\ v_\beta \\ v_0 \end{bmatrix} = \begin{bmatrix} \sqrt{2/3} & -1/\sqrt{6} & -1/\sqrt{6} \\ 0 & 1/\sqrt{2} & -1/\sqrt{2} \\ 1/3 & 1/3 & 1/3 \end{bmatrix} \begin{bmatrix} v_a \\ v_b \\ v_c \end{bmatrix} \rightarrow \mathbf{v}_T = \mathbf{T}_v \mathbf{v}_f \quad (3)$$

$$\begin{bmatrix} i_\alpha \\ i_\beta \\ i_0 \end{bmatrix} = \begin{bmatrix} \sqrt{2/3} & -1/\sqrt{6} & -1/\sqrt{6} \\ 0 & 1/\sqrt{2} & -1/\sqrt{2} \\ 1 & 1 & 1 \end{bmatrix} \begin{bmatrix} i_a \\ i_b \\ i_c \end{bmatrix} \rightarrow \mathbf{i}_T = \mathbf{T}_I \mathbf{i}_f \quad (4)$$

Transformation (1), (2) is conservative with respect to instantaneous power, namely

$$p = v_a i_a + v_b i_b + v_c i_c = v_\alpha i_\alpha + v_\beta i_\beta + v_0 i_0 = \mathrm{Re}\left(\mathbf{v}\mathbf{i}^*\right) + v_0 i_0 \quad (5)$$

Note that power conservation is a necessary condition for direct connection between different subsystems (e.g. three-phase star connection with single phase ground circuit) [29].

2.1.2. Impedances

Three-phase impedances (intended as Z(s) operators) are considered balanced, with equal phase impedances Z_f and mutual impedances Z_m, according to

$$\mathbf{Z}_3 = \begin{bmatrix} Z_f & Z_m & Z_m \\ Z_m & Z_f & Z_m \\ Z_m & Z_m & Z_f \end{bmatrix} \quad (6)$$

A graphic representation of (6) is shown in Figure 1. Note that the balanced impedance is not the more general case, and the transformation presented in the following can handle any impedance, being it balanced or not. Still, being this paper focused on DC faults, it is necessary to consider unbalanced impedances for the two-wire (DC) section, while phase-to-ground faults or other significant asymmetries in three-phase systems are not considered. Consequently three-phase impedances are assumed balanced for simplicity.

Considering the constitutive relation $\mathbf{v}_f=\mathbf{Z}_3\mathbf{i}_f$ and (3), (4), it is easy to prove that the transformed impedance $\mathbf{Z}_T$, defined according to $\mathbf{v}_T=\mathbf{Z}_T\mathbf{i}_T$, can be obtained according to

$$\mathbf{Z}_T = \mathbf{T}_v \mathbf{Z}_3 \mathbf{T}_I^{-1} = \begin{bmatrix} Z_f - Z_m & 0 & 0 \\ 0 & Z_f - Z_m & 0 \\ 0 & 0 & \dfrac{Z_f + 2Z_m}{3} \end{bmatrix} \quad (7)$$

Note that $\mathbf{Z}_T$ is diagonal due to the balanced form of $\mathbf{Z}_3$. Otherwise, non-diagonal terms are not null.

2.1.3. Connections

In the considered system, three-phase star connections represent the connection between a three-phase system and the ground (e.g. grounding of a transformer star-centre), represented by a single-wire system. Consequently, it is necessary to include three-phase star connections, as reported in Figure 2, in the presented modelling approach. Delta connection is not used in the system under analysis and hence not discussed, but it can be treated analogously. The three-phase star connection has four constitutive relations, namely

$$v_a = v_b = v_c = v_y, \quad i_a + i_b + i_c = i_y \quad (8)$$

Applying (1), (2) to (8), we obtain

$$\mathbf{v} = 0, \; v_0 = v_y, \; i_0 = i_y \quad (9)$$

which shows that a star connection is a short-circuit for the space vector, while it is a direct connection between the three-phase system zero component and the single-wire system. This result comes from the modified transformation introduced in (1), (2), and represents a significant simplification with respect to the standard transformation [30]-[33]. In fact, the traditional transformation would require an ideal transformer or, equivalently, a couple of controlled sources to connect zero-sequence and CM equivalent circuits [29]. In case of isolated star connection, being $i_y = 0$, the star connection is equivalent to a short-circuit for the space vector and an open-circuit for the zero component.

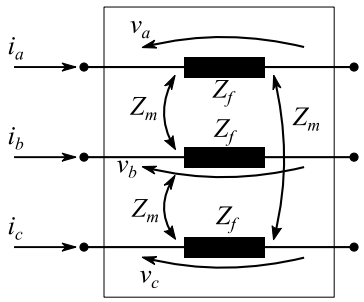

Figure 1 – Three-phase impedance $\mathbf{Z}_3$

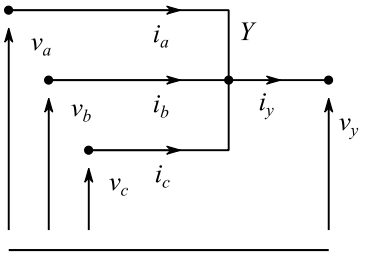

Figure 2 – Three-phase star connection

2.2. Two-wire transformation

2.2.1. Voltages and currents

Modal transformations are a general tool applied in different contexts [34], [35], which applies to the two-wire voltages v_+, v_- and currents i_+, i_-, resulting in DM and CM voltages and currents. A modified modal transformation is here introduced, namely:

$$v_{DM} = v_+ - v_-, \quad v_{CM} = \left(v_+ + v_-\right)/2 \tag{10}$$

$$i_{DM} = \left(i_+ - i_-\right)/2, \quad i_{CM} = i_+ + i_- \tag{11}$$

Note that, similarly to (1), (2), voltage and current transformation differ from each other. In matrix form, (10) and (11) can be rewritten as

$$\begin{bmatrix} v_{DM} \\ v_{CM} \end{bmatrix} = \begin{bmatrix} 1 & -1 \\ 1/2 & 1/2 \end{bmatrix} \begin{bmatrix} v_+ \\ v_- \end{bmatrix} \rightarrow \mathbf{v}_w = \mathbf{W}_v \mathbf{v}_l \tag{12}$$

$$\begin{bmatrix} i_{DM} \\ i_{CM} \end{bmatrix} = \begin{bmatrix} 1/2 & -1/2 \\ 1 & 1 \end{bmatrix} \begin{bmatrix} i_+ \\ i_- \end{bmatrix} \rightarrow \mathbf{i}_w = \mathbf{W}_I \mathbf{i}_l \tag{13}$$

Transformation (10), (11) is conservative with respect to instantaneous power, namely

$$p = v_+ i_+ + v_- i_- = v_{DM} i_{DM} + v_{CM} i_{CM} \tag{14}$$

2.2.2. Impedances

Two-wire impedances are considered in the general form

$$\mathbf{Z}_2 = \begin{bmatrix} Z_+ & Z_m \\ Z_m & Z_- \end{bmatrix} \tag{15}$$

A graphic representation of (15) is shown in Figure 3. Considering the constitutive relation $\mathbf{v}_l = \mathbf{Z}_2 \mathbf{i}_l$ and equations (12), (13) it is easy to prove that the transformed impedance $\mathbf{Z}_w$, defined as $\mathbf{v}_w = \mathbf{Z}_w \mathbf{i}_w$, can be obtained according to

$$\mathbf{Z}_w = \mathbf{W}_v \mathbf{Z}_2 \mathbf{W}_I^{-1} = \begin{bmatrix} Z_+ + Z_- - 2Z_m & \dfrac{Z_+ - Z_-}{2} \\ \dfrac{Z_+ - Z_-}{2} & \dfrac{Z_+ + Z_- + 2Z_m}{4} \end{bmatrix} \tag{16}$$

Note that a coupling between CM and DM is present when $Z_+ \neq Z_-$. To highlight this coupling in terms of equivalent circuits, the following hybrid formulation can be considered:

$$\begin{bmatrix} i_{DM} \\ v_{CM} \end{bmatrix} = \begin{bmatrix} \dfrac{1}{Z_{DM}} & -k \\ k & Z_{CM} \end{bmatrix} \begin{bmatrix} v_{DM} \\ i_{CM} \end{bmatrix} \tag{17}$$

where $Z_{DM} = Z_+ + Z_- - 2Z_m$, $Z_{CM} = (Z_+ Z_- - Z_m^2)/(Z_+ + Z_- - 2Z_m)$, $k = (Z_+ - Z_-)/2(Z_+ + Z_- - 2Z_m)$. Equation (17) allows building a significant equivalent circuit, where the coupling between DM and CM is represented by a suitable pair of controlled voltage and current sources, as reported in Figure 4.

2.2.3. Connections

In the considered system, two-wire star connections represent the connection between a two-wire system and the ground (e.g. DC middle point grounding), represented by a single-wire system. Consequently, it is necessary to include two-wire star connections, as reported in Figure 5, in the presented modelling approach. A two-wire star connection has three constitutive relations, namely

$$v_+ = v_- = v_y, \quad i_+ + i_- = i_y \tag{18}$$

Applying (10), (11) to (18), we obtain

$$v_{DM} = 0, \quad v_{CM} = v_y, \quad i_{CM} = i_y \tag{19}$$

which shows that a star connection is a short-circuit for the DM, while it is a direct connection between the two-wire system CM and the single-phase system. Similarly to the three phase case, this result comes from the modified transformation introduced in (10), (11). In case of isolated star connection, being $i_y = 0$, the star is equivalent to a short-circuit for the DM and an open-circuit for the CM.

2.3. Three-phase AC/DC Converter

Let us consider a three-phase, full-bridge VSC, as reported in Figure 6, being it the most common AC/DC converter. To obtain relationships in a general form, voltages are here referred to an arbitrary reference. In addition, let us assume

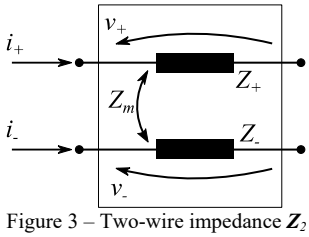

Figure 3 – Two-wire impedance $\boldsymbol{Z}_2$

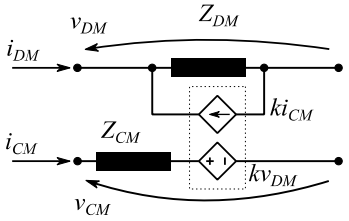

Figure 4 – Impedance equivalent DM/CM circuit

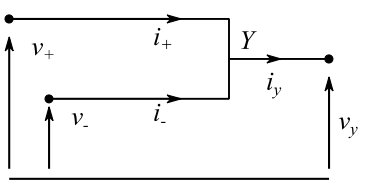

Figure 5 – Two-wire star connection

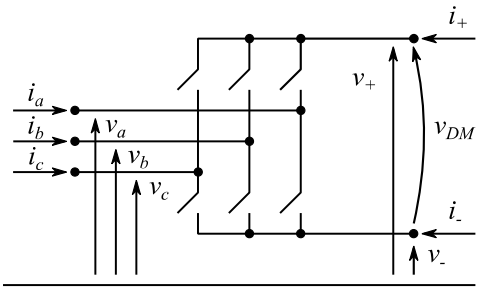

Figure 6 – Three-phase VSC

that the converter is working under controllability condition

$$v_- < v_a, v_b, v_c < v_+ \qquad (20)$$

The modelling approach presented in the following is based on power conservation: three-phase voltages are assumed to be independent variables imposed by the control, while other quantities are obtained as functions of independent variables by means of converter constraints. This approach is straightforward and does not depend on modulation techniques. Electrical variables reported in Figure 6 are transformed by means of (1), (2), (10), (11). The converter is subject to the following constraints: current null sum, which, from (2) and (11) results in

$$i_0 + i_{CM} = 0 \qquad (21)$$

and instantaneous power balance, which, from (5) and (14), leads to

$$\mathrm{Re}\left(\mathbf{vi}^*\right) + v_0 i_0 + v_{DM} i_{DM} + v_{CM} i_{CM} = 0 \qquad (22)$$

Since the lower level of the VSC control enforces the three AC voltages, the space vector **v** and zero component v_0 are considered as independent voltage sources. Being the switching logic usually referred to the DC middle point, it is useful to redefine the zero-component voltage source v_0' as referred to the DC middle point, resulting in

$$v_0' = v_0 - v_{CM} \qquad (23)$$

From the constraint (22) and considering equations (21), (23) it follows that

$$i_{DM} = -\frac{\mathrm{Re}\left(\mathbf{vi}^*\right) + v_0' i_0}{v_{DM}} \qquad (24)$$

The resulting equivalent circuit, which includes GSVEC and GZSEC and implements (21), (24), is reported in Figure 7. The proposed time-domain model is complete and includes switching ripple. However, if convenient, it can also be interpreted as an average-value model assuming the voltage sources **v** and v_0' as smooth variables with no switching ripple. In any case, the equivalent circuit can be solved when the independent sources are known, which in this case requires the knowledge of the voltage space vector and zero component.

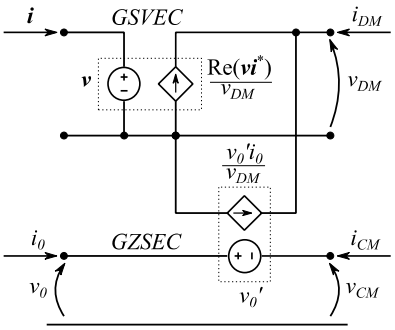

Figure 7 – Three-phase VSC GSVEC and GZSEC

All other quantities can be derived from independent sources and the network they are connected to.

2.4. DC/DC Converter

Let us consider a DC/DC converter, as reported in Figure 8. Similarly to Section 2.3, voltages are here referred to an arbitrary reference. By means of a modelling approach similar to the one used for three-phase converters, variables in Figure 8 are transformed by means of (10), (11). In addition, let us assume that the converter is working under controllability condition

$$0 < v_{H\,DM} < v_{DM} \qquad (25)$$

The converter is subject to the following current and power constraints

$$i_{CM} + i_{H\,CM} = 0 \qquad (26)$$

$$v_{DM} i_{DM} + v_{CM} i_{CM} + v_{H\,DM} i_{H\,DM} + v_{H\,CM} i_{H\,CM} = 0 \qquad (27)$$

An additional constraint recognized in Figure 8 is

$$v_- = v_{H-} \qquad (28)$$

From transformation (10) and constraint (28), we obtain

$$v_{HCM} = v_{CM} - v_{CM}' \qquad (29)$$

where v_{CM}' is defined as

$$v_{CM}' = \frac{v_{DM} - v_{H\,DM}}{2} \qquad (30)$$

From (29), considering constraints (26), (27), it is possible to

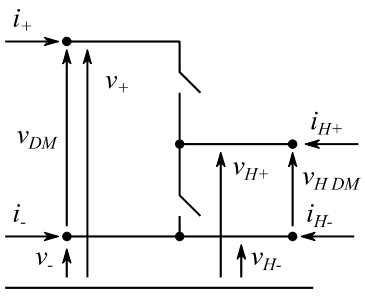

Figure 8 – DC/DC converter

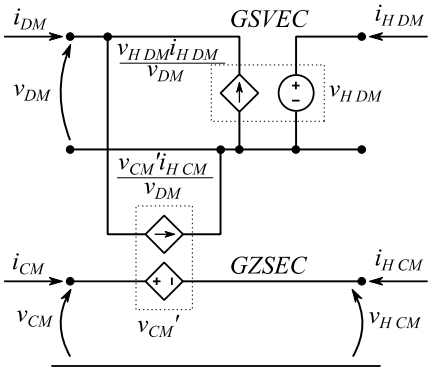

Figure 9 – DC/DC converter GSVEC and GZSEC

express the DM current as

$$i_{DM} = -\frac{v_{H\,DM}}{v_{DM}} i_{H\,DM} + \frac{v_{CM}'}{v_{DM}} i_{H\,CM} \tag{31}$$

Similarly to the VSC, the lower control level imposes the DM voltage $v_{H\,DM}$, hence represented as an independent voltage source. The CM voltage (30) is now indirectly imposed by the control from $v_{H\,DM}$ and the circuital constraint (28), resulting in a controlled voltage source. The GSVEC and GZSEC, which implements (26), (31), are reported in Figure 9.

3. Model Validation: Experimental Testing

To verify the effectiveness of the proposed equivalent circuits, an experimental setup has been realized in the DEIB PeDS Lab - Power electronics, electrical Drives and Storage systems Laboratory, Politecnico di Milano. The setup schematic is reported in Figure 10. The AC/DC converter is a standard, 3-leg, IGBT-based converter, whose main parameters are reported in Table 1, while the transformer parameters are reported in

Table 2. A resistor R_G was also introduced to emulated the resistance of the grounding loop (4 Ω or 42 Ω for testing purposes), while the load is represented by a 16 Ω resistor. The 42 Ω case allows appreciating a situation relatively close to no-load condition, and consequently a voltage similar to the no-load voltage which represents the voltage source driving leakage currents. Similarly, the 4 Ω case is a verisimilar working condition and allows appreciating a verisimilar ground current. The capacitors C_{leak}, equal to 1 µF, are added to emulate the capacitance to ground of a DC microgrid and to

Table 1 – AC/DC Converter Parameters

Parameter	Value
DC Voltage	200 V
Switching Frequency	10 kHz
Switching Inductance L_s	1 mH
AC Filter Capacitance C_{AC}	200 µF
DC Link Capacitance C_{DC}	6.8 mF

Table 2 – Transformer Parameters

Parameter	Value
Rated Power	20 kVA
Primary Line-to-line Voltage	400 V
Secondary Line-to-line Voltage	104 V
V_{cc}%	4 %
P_{CC}	400 W

provide a reclosing path for leakage currents.

The GSVEC and GZSEC of the setup depicted in Figure 10 is reported in Figure 11. The three-phase section is transformed by means of (1), (2), (7). The transformer is simply modelled as a trio of independent, sinusoidal, balanced voltage sources, resulting in the space vector $\boldsymbol{v}_T$, and series inductances L_T, neglecting magnetization. The transformer grounded star-centre and the star-connection of the filter capacitors C_{AC} are two occurrences or star connection (Figure 2), represented by means of (9). The VSC transformation is discussed in Section 2.3 and its model, reported in Figure 7, can be transferred to Figure 11. Note that, according to (7), the transformer series inductances and the converter switching inductances are simply divided by three in the GZSEC due to the absence of mutual terms. The DC section is transformed by means of (10), (11), (16). In particular, C_{DC} and R_{load}, directly connected between the DC poles, appear unchanged in the GSVEC, according to the trivial application of Figure 4. Capacitances C_{leak} are connected between the DC poles and ground, and their equivalent representation, obtained from Figure 4, appears in the GZSEC too. In these regards, one should recognize that the ground connection of the two capacitors is equivalent to a grounded two-wire star connection (Figure 5): consequently, capacitors appear in series between the DC poles on the GSVEC, while they appear in parallel on the GZSEC.

To better understand the methodology used to build the equivalent circuit reported in Figure 11, it must be recognized

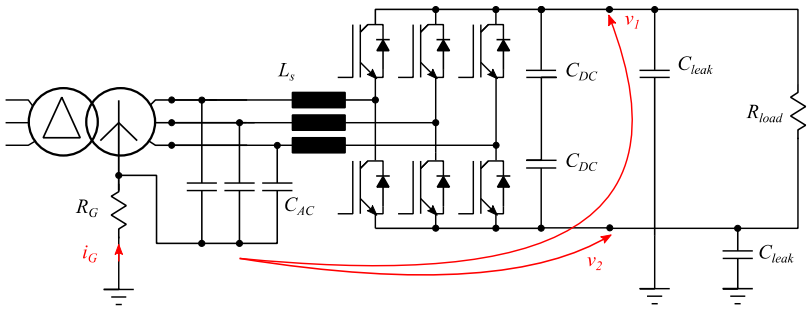

Figure 10 – AC/DC converter setup

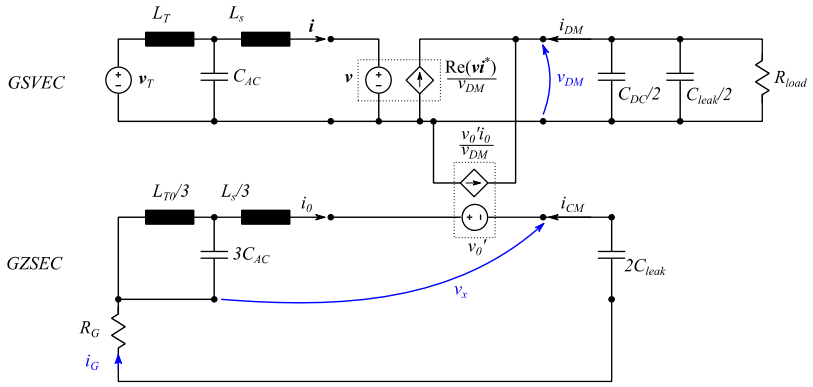

Figure 11 – AC/DC converter setup GSVEC (top) and GZSEC (bottom).

that the abovementioned three-phase (Figure 2, (9)) and two-wire (Figure 5, (19)) star connections cause a twofold effect. On the GSVEC, they impose null voltage on space-vectors and DM circuits, implying a short-circuit connections to a common reference point. Such set of conditions, together with reference point of the GSVEC part of VSC of Figure 7, is implemented by the short-circuit connection drawn in lower part of GSVEC in Figure 11, requested to impose a common zero point and to provide a return path for currents. On the contrary, the lower line sketched in GZSEC is the physical, not transformed ground network, directly connected with the star points of the abovementioned star connections. Consequently, in the upper part of GZSEC the CM transformed currents take place, while in the lower part of GZSEC the physical ground currents are present. Lastly, note that, due to the modified transformation introduced in this paper, the ground current i_G is the same both in the physical and in the equivalent circuit.

To evaluate the accuracy of the proposed GSVEC and GZSEC, significant quantities to be checked are the DC poles voltages with respect to the transformer star center v_1, v_2 and the system ground current i_G, as highlighted in red in Figure 10. The corresponding quantities in and GZSEC are the voltage v_x and the current i_G, highlighted in blue in Figure 11. The direct measurement of v_x is clearly not possible, but it is obtained from measures of v_1, v_2 by means of (10), resulting in

$$v_x = \frac{v_1 + v_2}{2} \qquad (32)$$

The simulated voltage v_x requires a bit more elaboration. The theoretical zero-sequence voltage source v_0' can be easily calculated considering each phase switched voltage produced by standard PWM modulation and (1). Since the considered circuit is linear but voltage sources are non-sinusoidal, the steady-state circuit analysis is performed in frequency domain. Consequently, the zero-sequence voltage source v_0' is transformed from time domain to frequency domain through Fourier transform. Note that, since the converter duty cycle has a fundamental frequency equal to 50 Hz, the zero-sequence voltage source v_0' is evaluated over an integer number of periods of the fundamental frequency. However, in the following, much smaller time intervals will be shown to be able to appreciate the waveforms at switching frequency. Additionally, it is worth considering that the waveforms change cyclically every 20 ms according to the fundamental frequency. Considering now the simulated ground current i_G, it can be obtained from the no-load zero-sequence voltage v_0' and the GZSEC impedance. The calculation of the impedance of

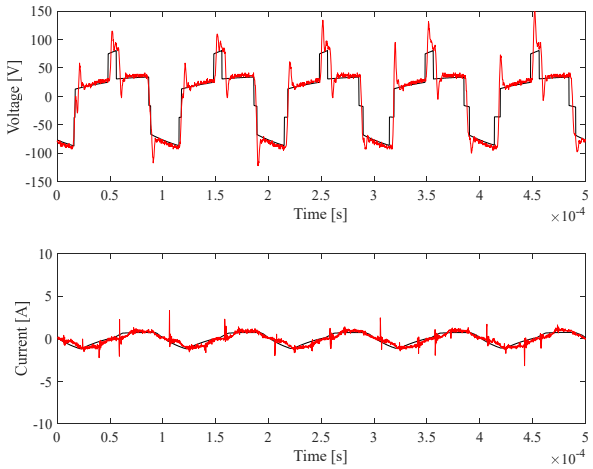

Figure 12 – CM voltage v_x (top) and current i_G (bottom) with 42 Ω ground resistor: calculated (black) vs measured (red)

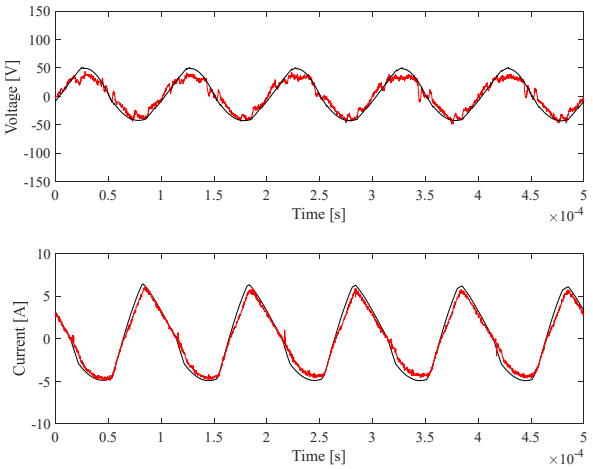

Figure 13 – CM voltage v_x (top) and current i_G (bottom) with 4 Ω ground resistor: calculated (black) vs measured (red)

TABLE 3 – AC/DC CONVERTER PARAMETERS

Parameter	Value
DC Voltage	400 V
Switching Frequency	10 kHz
Switching Inductance L_s	1 mH
AC Filter Capacitance C_{AC}	200 µF
DC Link Capacitance C_{DC}	6.8 mF

TABLE 4 – TRANSFORMER PARAMETERS

Parameter	Value
Rated Power	160 kVA
Primary Line-to-line Voltage	20 kV
Secondary Line-to-line Voltage	225 V
V_{cc}%	4 %
P_{CC}	2350 W

the circuit reported in Figure 11 is straightforward. Once that the ground current i_G is known, the voltage v_x can be evaluated. The time-domain waveform of voltage v_x is then derived by inverse Fourier transform.

The comparison between measured and calculated quantities is reported in Figure 12 for the 42 Ω case and in Figure 13 for the 4 Ω case. Comparing the measured and calculated quantities, it is possible to observe that the proposed equivalent circuit provides good accordance with the experimental results.

4. GENERALIZED SPACE-VECTOR AND ZERO-SEQUENCE EQUIVALENT CIRCUITS APPLICATIONS

To show the effectiveness of the proposed approach, an example DC microgrid is chosen as a test case. The considered microgrid schematic is reported in Figure 14. The AC/DC converter and transformer parameters are reported in Table 3 and Table 4. In Figure 14, the bold lines represent a DC line realized with a cable, whose parameters are reported in Table 5. The PV plant parameters are reported in Table 6, while the DC/DC converters parameters are reported in Table 7. Line impedances and capacitance to ground and PV panel capacitances to ground are not explicitly included in Figure 14 for simplicity. Depending on the state of the switch S_G,

TABLE 5 – DC LINE PARAMETERS

Parameter	Value
Cable type and section	4-pole, PVC insulated, 150 mm^2
Per-length resistance	0.061 Ω/km
Per-length line inductance	0.118 mH/km
Per-length line susceptance	201 µS/km
Length	0.30 km

TABLE 6– PHOTOVOLTAIC PLANT PARAMETERS

Parameter	Value
Peak power	100 kW
No-load voltage	800 V
Module surface	1 m^2
Module efficiency	18 %
Module number	695

TABLE 7– DC/DC CONVERTERS PARAMETERS

Parameter	Value
Switching Frequency	10 kHz
Switching Inductances $L_{s\,PV}$, $L_{s\,ESS}$	1 mH
Filter Capacitance $C_{DC\,PV}$, C_{ESS}	200 µF
DC Link Capacitances $C_{DC\,ESS}$, C_{PV}	6.8 mF

reported in Figure 14, the considered microgrid can represent different cases of practical interest. Examples can be recognized in public distribution systems for grounded systems, or in industrial distribution systems in case of isolated systems.

The main applications of GSVEC and GZSEC for DC microgrids analysis are the evaluation of leakage and ground fault current. With respect to direct simulation, the equivalent circuit approach has some noticeable advantages. Firstly, it greatly simplifies the problem when the zero-sequence phenomena are limited, and coupling effects on the GSVEC are negligible. In this case, it is possible to assume GSVEC working at rated conditions, so as not to be explicitly solved. Hence GZSEC is analytically solved or numerically simulated, given some external generators obtained from GSVEC. This

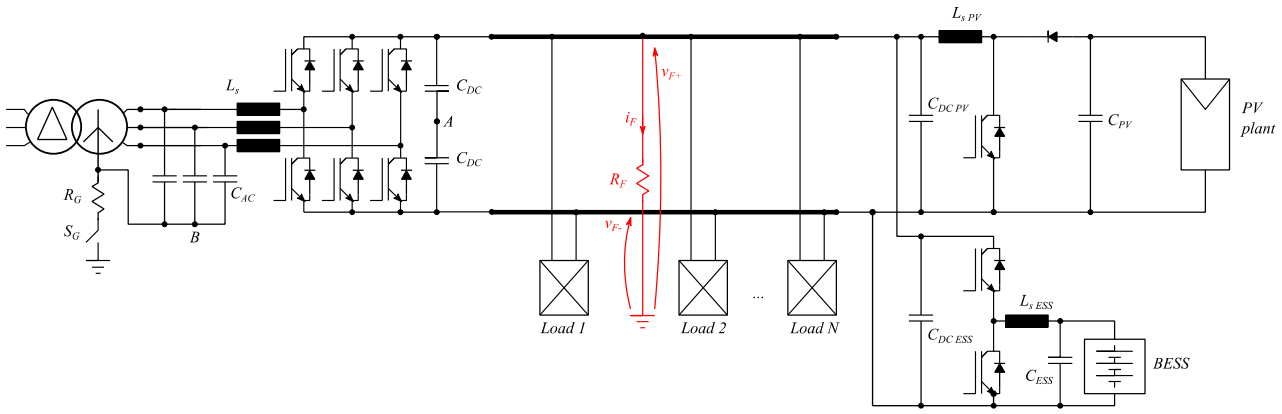

Figure 14 – DC microgrid electric diagram. Red portion is to be considered for ground fault analysis only.

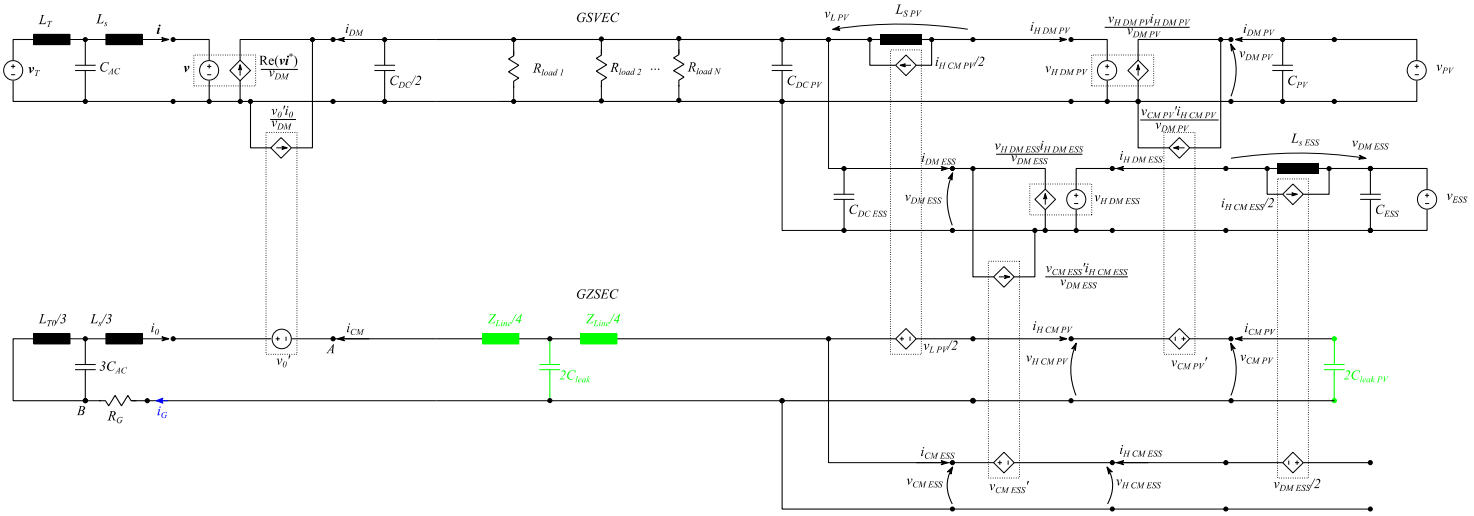

Figure 15 – DC microgrid equivalent circuit for leakage current evaluation: GSVEC (top) and GZSEC (bottom). Line impedance and capacitance to ground and PV leakage capacitance, needed for leakage current evaluation, are highlighted in green.

greatly simplifies both frequency-domain analysis and time-domain dynamic system solution. Secondly, the equivalent circuit provides clear indications on the parameters which most affect the phenomena under analysis, highlighting possible mitigation strategies. Additionally, explicit knowledge of the actual equivalent circuit is necessary to forecast some critic situations, such as LC resonances.
In the following, the targets addressed are leakage and ground fault current evaluation in system with grounded transformer. A case study in AC-isolated power systems is also considered, highlighting DERs contribution to fault currents.

4.1. Leakage Currents in systems with grounded transformer

Leakage currents at switching frequency are a well-known issue in hybrid power systems, but still represent a partially unsolved problem. In fact, different countermeasures to reduce leakage currents are known, but a systematic approach for leakage currents evaluations is lacking. However, to correctly address this issue, it is necessary to estimate leakage current amplitude first.

The GSVEC and GZSEC of our test-case DC microgrid, assuming the switch S_G to be closed, are reported in Figure 15, except from the red portion of Figure 14, which is to be considered successively for ground fault analysis. The main blocks, such as balanced impedances, AC/DC and DC/DC converters and star connections can be recognized from figures and discussion reported in Sections 2 and 3. Additionally, note the coupling due to the DC/DC converters switching inductances: being unbalanced impedances (just one inductance on the positive pole, no inductance on the negative pole), the equivalent circuit, according to Figure 4, includes an inductance in parallel with a controlled current source on the GSVEC, and a controlled voltage source on the GZSEC.

Note also that line impedance and capacitance to ground and PV capacitance to ground, not included for simplicity in Figure 14, are included in the GZSEC reported in Figure 15 and highlighted in green, being fundamental for leakage current evaluation. In particular, the line is modelled by means of one T section, whose parameters are derived from the line parameters reported in Table 5. The PV plant leakage capacitance depends significantly on the specific PV panel technology, but for the purposes of this paper it can be considered, on average, roughly equal to 1 nF per module [36], [37], resulting in an overall capacitance $C_{leak\,PV}$ = 695 nF. On the GSVEC reported in the same figure, these parameters do not produce a significant effect, and are hence not included for simplicity.

Considering the GZSEC reported in Figure 15, firstly it is worth noting that the ESS and its DC/DC converter do not contribute to leakage current since their active parts are isolated from ground and ESS capacitance to ground is usually negligible. Accordingly, the corresponding isolated star connection results in an open circuit on the GZSEC. One can hence recognize that the leakage current is driven by three sources: CM voltage source $v_{CM\,PV}$', controlled voltage source $v_{L\,PV}/2$, and zero-sequence voltage source v_0'. Additionally, three reclosing paths are possible: through the AC section grounding arrangement, through the DC line capacitance to ground and through the PV panels capacitance to ground.

The only current which is possible (and meaningful) to measure directly is the ground current i_G, being other reclosing paths represented by distributed capacitances. To highlight the equivalent circuit effectiveness, some considerations on this current are drawn. Firstly, it can be recognized that the controlled voltage sources relative to the DC/DC converter and its switching inductance are in series with a capacitor, such that their DC component has no effect on steady-state current, which, consequently, contains only components at switching frequency. It is also recognized that the filter capacitors C_{DC} and $C_{DC\,PV}$ included in the GSVEC are practically a short circuit for current components at switching frequency. Under this condition and in steady-state, it is possible to assert that the controlled current sources on the GSVEC, representing the interaction with the GZSEC, do not alter any voltage. Consequently, the GSVEC can be solved first, neglecting coupling. The GZSEC is then solved considering the controlled

voltage sources as independent voltage sources, whose value is obtained from the GSVEC. Therefore, the voltage sources v_0', $v_{L\ PV}/2$ and $v_{CM\ PV}$' are imposed by converters modulation algorithms under rated steady-state conditions.

The voltage source $v_{L\ PV}/2$, due to unbalanced switching inductance L_{sPV}, deserves further discussion. In GSVEC, since filter capacitors C_{DC} and $C_{DC\ PV}$ are practically a short-circuit at switching frequency, the high-frequency ripple on the voltage $v_{H\ DM}$ is totally contained in the voltage drop $v_{L\ PV}$. Consequently, the voltage source $v_{LPV}/2$ produces a voltage equal to - $v_{HDM}/2$ (high-frequency components only). Because of (31), the voltage source $v_{CM\ PV}$' holds just the same high-frequency content, descending from $v_{H\ DM}$. This leads to the conclusion that unbalanced switching inductances in DC/DC converters double the high-frequency voltage driving leakage currents. This result opens the way to further discussion on the possible advantage of splitting switching inductances on the two conductors. These considerations, however, lie outside the purposes of this paper.

Another issue worth considering is that, when different converters are included in one system, switching frequency may be different from converter to converter and, even if the switching frequency is the same, the relative phase of each converter switching is randomised since converters switching is usually not synchronized. In this paper, all converters switching frequency are assumed equal to 10 kHz (see Table 3, Table 7) and the phase shift corresponding to the worst-case ground current is applied.

The leakage current i_G is simulated assuming the resistance of the grounding arrangement R_G equal to 2 Ω. The results are reported in Figure 16, where the AC/DC and PV converters current contributions, calculated via superposition, are highlighted. One can notice that the leakage current reaches significant values, with a peak value roughly equal to 20 A. Additionally, even though the waveform slightly changes inside the 20 ms period, the current peak-to-peak amplitude is almost constant. This may or may not be considered acceptable depending on the specific application, but it is wise to consider possible solutions to limit the leakage current amplitude.

Considering the GZSEC reported in Figure 15, one can theoretically act in two ways to reduce leakage current: reducing the capacitances to ground of the line and PV or, alternatively, addressing the voltage sources driving leakage currents. Reducing capacitances to ground is not practically feasible. With regards to voltage sources, the effect of the voltage source v_0' can be easily mitigated by connecting the DC middle point with the AC system star-centre, which corresponds to a short circuit between the nodes A and B on the GZSEC reported in Figure 14 and Figure 15. If this solution is adopted, the AC/DC converter still produces a zero-sequence current, which is, however, restrained in the connection between the AC system star-centre and DC middle point, not affecting grounding arrangements. This is not a complete solution to the problem, but it makes it much more controllable and allows to avoid most significant issues related to zero-sequence currents driven by AC/DC converters: in fact, in this case the zero-sequence current is restrained in a small area, possibly included in the converter switchgear, and does not affect the whole system. However, leakage currents are still present in the system, driven by the controlled voltage sources representing the PV DC/DC converter and reclosing through the line and PV capacitances to ground. In order to further reduce leakage currents, it is possible to use an isolated DC/DC converter in place of the standard DC/DC converter depicted in Figure 14. The introduction of the isolated DC converter will practically open the GZSEC, avoiding leakage currents affecting line and PV capacitances to ground. Further discussion on these possible solutions, however, lies outside the purposes of this paper.

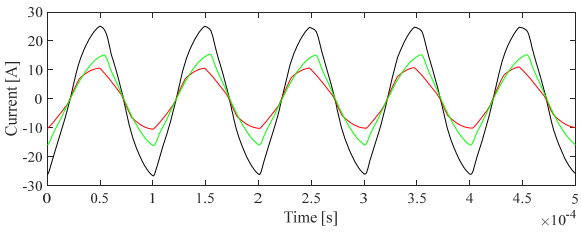

Figure 16 – Leakage current i_G: total ground current (black), AC/DC converter contribution to ground current (red) and PV contribution to ground current (green).

4.2. *Ground fault currents in systems with grounded transformer*

The GSVEC and GZSEC for ground fault evaluation are reported in Figure 17 and, in this Section the switch S_G must be considered closed. As highlighted in Figure 14, a PGF affecting the positive pole is considered. A PGF affecting the negative pole can be treated analogously.

The main circuit blocks can be recognized from discussion reported in Section 4.1. Note that, similarly, line impedance and capacitance to ground and PV capacitance to ground, not included for simplicity in Figure 14, are included in the GZSEC reported in Figure 17 and highlighted in green. On the GSVEC reported in the same figure, these parameters do not produce a significant effect, and are hence not included for simplicity. The line is modelled by means of two T sections, whose parameters are derived from the line parameters reported in Table 5. The term h appearing in line impedances in Figure 17 represents the ratio between the distance of the fault from the AC/DC converter and the total line length, so that $0 < h < 1$.
Additionally, note the coupling between GSVEC and GZSEC due to the fault, highlighted in red. Being the fault represented as an unbalanced impedance (one resistor connecting the positive pole with ground, see Figure 14), the equivalent circuit is deduced from the general circuit in Figure 4 under the conditions $Z_+=R_F$, $Z_-=\infty$, $Z_m=0$. It includes a controlled current source on the GSVEC, and a controlled voltage source, in series with the fault resistance, on the GZSEC.

For ground fault current evaluation, some significant simplifications apply. Firstly, similarly to the preceding analysis of leakage currents, it can be assumed that the controlled current sources appearing in GSVEC and representing the interaction with the GZSEC do not noticeably affect the GSVEC voltage levels. This hypothesis can be

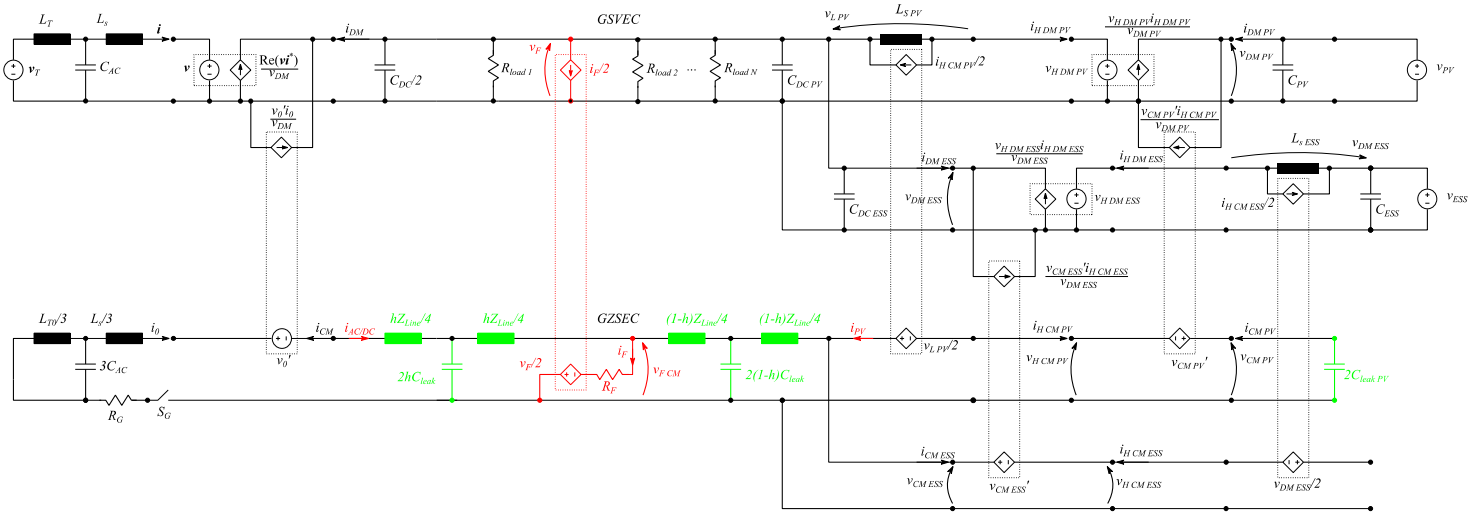

Figure 17 – DC microgrid equivalent circuit for ground fault current evaluation: GSVEC (top) and GZSEC (bottom). The ground fault equivalent circuit is highlighted in red. Line impedances and capacitances to ground and PV leakage capacitance, needed for ground fault current evaluation (including transient), are highlighted in green.

verified a posteriori and allows solving the GZSEC only, considering the controlled voltage sources as independent voltage sources, whose value is imposed by the GSVEC. Consequently, the GZSEC becomes a linear system subject to a number of external voltage sources. By superposition, the aperiodic component of the fault current is calculated considering only voltage sources DC components, which are present only in $v_F/2$ and $v_{CM\,PV}$'. It is worth nothing that leakage currents are still present in the system, and can be evaluated according to the procedure described in Section 4.1 considering high-frequency voltage components only. Note also that the controlled voltage source $v_{CM\,PV}$' is in series with a capacitor, such that its contribution to steady-state fault current is null. This implies that the steady-state fault current is driven by voltage source $v_F/2$, which represent the main DC voltage, and recloses through the transformer grounding arrangement. Consequently, only the AC/DC converter feeds the fault current in steady state.

In the perspective of using the proposed equivalent circuits for protection design, it is of interest to solve the GSVEC and GZSEC reported in Figure 17 considering the fault transient. This allows determining the steady-state fault current and the fault current peak; additionally, being the GSVEC voltages assumed not to be affected by the ground fault, the same circuit allows determining the positive and negative poles voltages in the fault section (Figure 14). In fact, once that the voltage in a section of the GZSEC is known from the circuit solution, pole voltages can be derived by inversion of (10), (11), resulting in

$$\begin{aligned} v_{F+} &= v_{F\,CM} + v_F/2 \\ v_{F-} &= v_{F\,CM} - v_F/2 \end{aligned} \tag{33}$$

It is often stated that the fault current peak is large and due to capacitor discharge. However, in the considered test microgrid, being the DC mid-point isolated from ground, the large filter capacitors are not involved in the fault transient, but only line capacitance to ground and PV leakage capacitance are. Additionally, it is reasonable to assume a grounding resistance equal to 2 Ω for the transformer grounding arrangement, while for the fault resistance can be reasonably assumed equal to 10 Ω. Consequently, the fault transient is expected to be significantly damped.

The circuit solution can be obtained in different ways. Firstly, it is possible to solve the system of 10 differential equations (4 capacitors + 6 inductors in the GZSEC), manually or by means of a suitable software. Alternatively, it is possible to simulate the GZSEC only in a circuit solver. This proves to be an easy task, which can be performed by simple (and freely available) software tools, such as SPICE solvers, since the circuit includes only constant sources and passive elements. On the contrary, as mentioned in the Introduction, the study of ground fault currents in the original systems, without the proposed equivalent circuit, would require the simulation of the whole system, including power electronics and related controls, which would require more sophisticated software solutions, not always available nor commonly used by professional operators. The results presented in the following are obtained from simulations of the GZSEC only, realised in Simulink.

The ground fault current i_F and its contribution from the AC/DC converter ($i_{AC/DC}$, Figure 17) and PV(i_{PV}, Figure 17) are calculated for the considered test microgrid in case of faults at two different points along the line. Additionally, the voltage in the fault section of the GZSEC $v_{F\,CM}$ (Figure 17) is evaluated, and the corresponding pole voltages v_{F+}, v_{F-} (Figure 14) are hence calculated from (33). The results are reported in Figure 18 and Figure 19. One can note that, even though the current transient exhibits significantly different shapes, the fault position does not affect significantly the peak current nor the steady-state current. This confirms that line parameters produce minor effects on fault currents and that the main parameters affecting the fault transient are the AC/DC converter reactive elements, the PV leakage capacitance and the fault resistance. Additionally, one can note that the peak ground fault current is not much larger than steady-state fault current (20 A peak vs 16.67 A steady-state) and that, while the AC/DC converter alone feeds the fault in steady-state, the PV and its converter

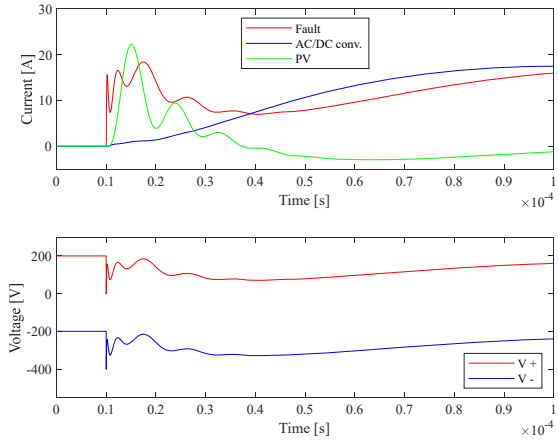

Figure 18 – Ground fault currents in grounded systems (top): fault current i_F (red), AC/DC converter fault current contribution $i_{AC/DC}$ (blue) and PV converter fault current contribution i_{PV} (green). DC poles voltages in the fault section in grounded systems (bottom): positive pole voltage (red) and negative pole voltage (blue). All quantities are calculated in case of ground fault at 30 m from the FEC (h = 0.1).

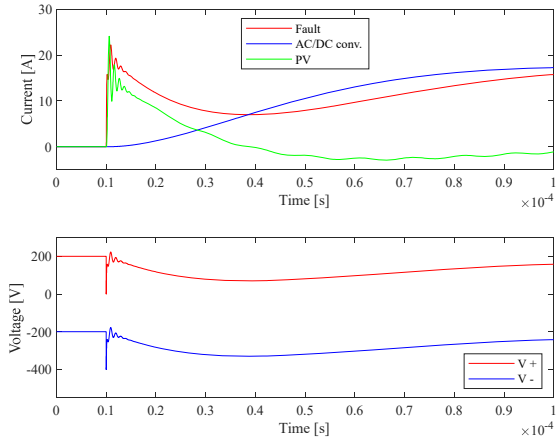

Figure 19 – Ground fault currents in grounded systems (top): fault current i_F (red), AC/DC converter fault current contribution $i_{AC/DC}$ (blue) and PV converter fault current contribution i_{PV} (green). DC poles voltages in the fault section in grounded systems (bottom): positive pole voltage (red) and negative pole voltage (blue). All quantities are calculated in case of ground fault at 270 m from the FEC (h = 0.9).

provides almost the whole peak current. Lastly, one can note that the poles voltages are affected by a significant voltage perturbation, whose amplitude is of the same order of magnitude of the pole-to-pole voltage.

Some remarks on fault currents are worth: firstly, similarly to ground faults in AC systems, the fault current is significantly smaller that the line rated current (100 kW / 400 V = 250 A). Secondly, one should consider that the leakage current is still significant during faults, so that the fault current will present a DC component superimposed with non-negligible high-frequency components, similar to the leakage current considered in Section 4.1. To exemplify this issue, the AC/DC converter fault current contribution $i_{AC/DC}$, calculated in case of ground fault at 270 m from the FEC (h = 0.9) and including leakage current, is reported in Figure 20. This current is

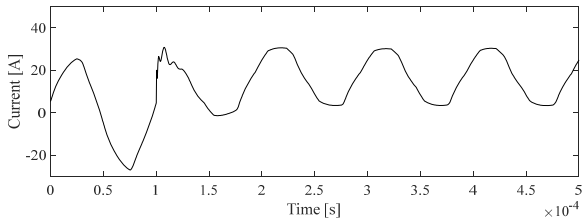

Figure 20 – Ground fault currents in grounded systems: AC/DC converter fault current contribution $i_{AC/DC}$, including leakage current, calculated in case of ground fault at 270 m from the FEC (h = 0.9).

particularly significant because it is the one seen by protection devices installed in the AC section or in the DC section at the AC/DC converters terminals. Note that the leakage current waveform changes before and after the fault: in fact, the leakage current before the fault is calculated from the circuit reported in Figure 17, excluding the red portion representing the fault, while the leakage current after the fault is calculated from the same circuit including the fault.

With regards to the steady-state fault current, one can note that it is driven by the controlled generator $v_F/2$ representing the fault and is limited by circuit resistances only. With the considered values for grounding resistance (2 Ω) and fault resistance (10 Ω), the line resistance (< 20 mΩ) is clearly negligible, and, consequently, the steady state fault current is simply obtained as

$$i_G = \frac{V_F / 2}{R_G + R_F} \qquad (34)$$

Assuming that the voltage in the fault section V_F remains close to the system rated voltage (400 V), which is reasonable since the converter is expected to maintain controllability during ground fault, the fault current results in i_G = 16,67 A, which is consistent with GZSEC circuit simulation.

4.3. Ground fault currents in systems with isolated transformer

The GSVEC and GZSEC for ground fault evaluation are reported in Figure 17, where the switch S_G must be considered open. As highlighted in Figure 14, a PGF affecting the positive pole is considered, but a fault affecting the negative pole can be treated analogously.

Firstly, the same consideration developed in Section 4.2 regarding equivalent circuit derivation, possible simplifications and circuit solution apply. However, in case of an isolated transformer, fault resistance R_F is assumed equal to 2 Ω.

As discussed in Section 4.2, it is of interest to solve the GSVEC and GZSEC reported in Figure 17 considering the fault transient. In this case, being the transformer isolated from ground, the steady-state fault current is clearly null. However, it is known that isolated systems can be subject to significant transitory currents and voltage oscillations in case of ground faults. The ground fault current and pole voltages in the fault section are hence calculated for the considered test microgrid in case of faults at two different points along the line, and the

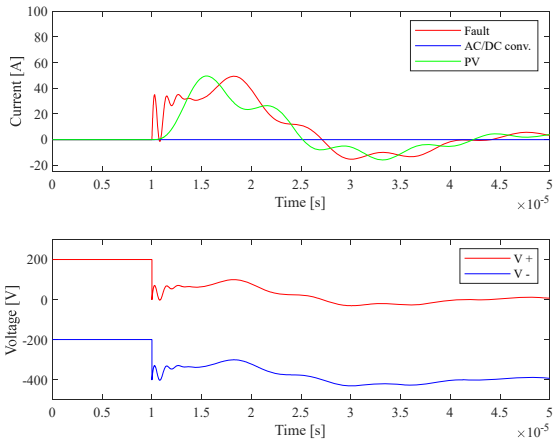

Figure 21 – Ground fault currents in isolated systems (top): fault current i_F (red), AC/DC converter fault current contribution $i_{AC/DC}$ (blue) and PV converter fault current contribution i_{PV} (green). DC poles voltages in the fault section in isolated systems (bottom): positive pole voltage (red) and negative pole voltage (blue). All quantities are calculated in case of ground fault at 30 m from the FEC (h = 0.1).

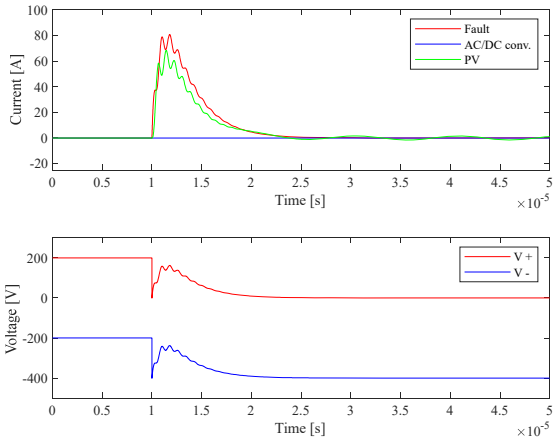

Figure 22 – Ground fault currents in isolated systems (top): fault current i_F (red), AC/DC converter fault current contribution $i_{AC/DC}$ (blue) and PV converter fault current contribution i_{PV} (green). DC poles voltages in the fault section in isolated systems (bottom): positive pole voltage (red) and negative pole voltage (blue). All quantities are calculated in case of ground fault at 270 m from the FEC (h = 0.9).

results are reported in Figure 21 and Figure 22. One can note that, as expected, the steady-state pole voltage of the faulty pole is null, while the steady-state voltage of the healthy pole is equal to the line-to-line voltage. The pole voltages also exhibit some oscillations, whose amplitude, however, is not very significant. This can clearly change drastically in different systems (e.g. different line length or cable physical properties), but the proposed equivalent circuits allow simple evaluation of the phenomenon under different condition. Considering now the fault current, one can note that the transient amplitude and duration varies significantly with respect to the fault position along the line. This is reasonable in isolated systems, where the fault current is mainly determined by line reactive parameters. One can also note that the fault current peak in case of isolated system is significantly larger than the one obtained in grounded systems (see Figure 18, Figure 19), which is not common. Additionally, this current is almost completely provided by the PV leakage capacitances and flows through the PV DC/DC converter, while the AC/DC converter does not provide a significant contribution. While these results may vary depending on the line modelling approach and/or on system parameters, they highlight that the proposed approach based on equivalent circuits provide a useful tool to study many possible system configurations in a simple and direct way.

5. Considerations on Protection Design

As highlighted in the previous Sections and according to simulations results, if the MV/LV transformer neutral point is grounded and not connected to the converter DC midpoint, there is a current flowing through the ground even in absence of ground faults. RCDs are commonly used for ground fault detection in systems where the prospective ground fault current is not so high to cause the short circuit protection tripping, which is the case of the systems here discussed. However, because of the aforementioned ground current, unwanted RCD trips may occur. In particular, if an RCD is installed on the AC connection between the transformer and the converter, a trip creates a shutdown of the whole system during normal operation. Even if a source ground return current sensor (i.e. a toroid) is installed on the grounding connection of the transformer star-centre, nuisance trips occur.

On the contrary, if the converter DC midpoint is connected to the transformer star-centre, RCDs work correctly as long as the cable/bus-bar connection between the midpoint and the star-centre is included in the residual current detection. Consequently, the connecting system has to go through the RCD toroid or a high frequency current sensor has to be installed on the connecting system to detect the related circulating current and to sum it with the currents in the AC phases. In addition, the source ground return current sensor works properly, since the currents generated during the normal operation do not flow through the grounding connection of the transformer star-centre anymore.

In case of ground fault on the DC side (in particular through the grounded DC exposed conductive parts), a steady-state DC component (fault current) is superimposed on the oscillating component at switching frequency (leakage current). It is not a problem, as long as an RCD type B is installed on AC side. In the RCD type B, while still using a single toroid, a special method of operation and measure is used for the detection of DC fault currents [38]. The toroid is no more used passively, by reading only the current induced as in the case of types AC and A, but the toroid itself is fed by a voltage with a waveform of kHz frequency. This voltage source is an oscillator, which is connected to the AC system voltage. The voltage waveform generates in the winding on the toroid an alternating current at the same frequency also in absence of ground fault. A resistance in series with the winding creates a voltage drop, whose value is sent to a microprocessor including a low-pass filter. If there is a residual current higher than the threshold set, it causes the core saturation and the consequent variation of the waveform of the current flowing through the resistance. Thanks to the low-pass filter it will be possible to detect also the DC fault component, even if it superimposed on the oscillating component at switching frequency.

Another way to avoid unwanted trips could be the use on the DC side of a new RCD concept, able to distinguish between a leakage current (without DC component) and a ground fault current (with DC component) [39]. If there is no DC component and the leakage current peak exceeds the set threshold, a warning signal is generated (not a tripping signal), which is indicative of an anomalous operating condition, possibly requiring a maintenance intervention. Instead, if a DC component exceeding the set threshold is detected, a tripping signal is generated, indicating the ground fault condition.

Regarding the DC ground fault location and the related selectivity, if a ground fault occurs on the main DC line, an already existing RCD type B installed on the AC side is able to detect such ground fault, but the protection trip affects the whole DC system. On the contrary, if a ground fault occurs on a DC feeder connecting the main line with loads, coordination of the feeder and main protections is required to guarantee the system selectivity and the service continuity, avoiding the unnecessary loss of supply to other healthy feeders. Such coordination can be achieved, for example, by installing RCDs on each feeder and on the main DC bus and performing time-current based or logic-based coordination. Note that this DC RCDs have to be able not only to detect a DC ground fault current, but also to be DC supplied.

On the other hand, if the MV/LV transformer is owned by the End User, the neutral point can be ungrounded, while the DC exposed conductive parts are still grounded. In this case, there isn't a reclosing path for the steady-state ground fault current. Nevertheless, during a ground fault, there is still a transient fault current, as shown in the Section 4.3, passing through the PV and line parasitic capacitances. Since such a transient current doesn't reclose through the transformer, an RCD installed on the AC side isn't affected.

Besides, compared to the previous scenario, in this case there isn't a leakage current affecting the AC/DC converter or AC transformer during normal operation. Hence, by using the new RCD concept installed on the DC side, even if there isn't a steady-state current during a ground-fault, the transient ground fault current can generate a warning signal. In this scenario, such a warning signal is the result of an occurred transient ground fault.

6. Conclusion

Hybrid AC/DC distribution systems are becoming reality and, while they present many advantages over traditional AC power systems, further studies on protection from DC faults and protection devices requirements are needed. In particular, two aspects of the aforementioned systems are not completely covered in literature from a methodological perspective. The first aspect is the evaluation of ground fault currents in hybrid AC/DC distribution systems with high fault-loop impedance. The second aspect is the evaluation of high-frequency leakage currents which can flow through grounding arrangements due to the oscillations of the DC poles voltages towards ground caused by converters switching.

In this paper, a new method for ground fault and leakage currents evaluation in hybrid power systems including DERs is introduced. The proposed method is based on equivalent circuits built by generalization of traditional space-vector and zero-sequence circuits used for AC system analysis. This method, validated by means of experimental tests, allows building an equivalent circuit of the whole hybrid system, including AC sections, DC sections, ground return path and power converters. It also allows simple evaluation of both steady-state and transient fault currents, which represent the fundamental requirement for protection design. The presented case study allows appreciating the versatility of the proposed approach with respect to traditional simulation method, which require software solutions not always available nor commonly used by professional operators. Additionally, the proposed method clearly highlights the effect of circuit parameters on ground fault and leakage currents. The presented results allow drawing some considerations on protection devices requirements, necessary to obtain correct operation in hybrid AC/DC distribution systems.

References

[1] DIRECTIVE RED II - Revision of Directive (EU) 2018/2001 of the European Parliament and of the Council of 21 December 2018.

[2] Abner Ramirez, Uriel Vargas, Mohamed A. Abdel-Rahman, Lumped-parameters equivalent of a photovoltaic system for load flow analysis, Renewable Energy, Volume 170, 2021, Pages 163-171.

[3] Shinong Wang, Huan Luo, Yuan Ge, Shilin Liu, A new approach for modeling photovoltaic modules based on difference equation, Renewable Energy, Volume 168, 2021, Pages 85-96.

[4] Divine Atsu, Istvan Seres, Mohammadreza Aghaei, Istvan Farkas, Analysis of long-term performance and reliability of PV modules under tropical climatic conditions in sub-Saharan, Renewable Energy, Volume 162, 2020, Pages 285-295.

[5] Ping Wang, Meiya Kong, Wei Du, Linhong Wang, Lei Ni, The effect of pollutants on leakage current and power degradation of photovoltaic modules, Renewable Energy, Volume 146, 2020, Pages 2668-2675

[6] H.I. Dag, M.S. Buker, Performance evaluation and degradation assessment of crystalline silicon based photovoltaic rooftop technologies under outdoor conditions, Renewable Energy, Volume 156, 2020, Pages 1292-1300.

[7] Gianfranco Di Lorenzo, Sara Rotondo, Rodolfo Araneo, Giovanni Petrone, Luigi Martirano, Innovative power-sharing model for buildings and energy communities, Renewable Energy, Volume 172, 2021, Pages 1087-1102.

[8] Mostafa Kermani, Behin Adelmanesh, Erfan Shirdare, Catalina Alexandra Sima, Domenico Luca Carnì, Luigi Martirano, Intelligent energy management based on SCADA system in a real Microgrid for smart building applications, Renewable Energy, Volume 171, 2021, Pages 1115-1127.

[9] U.G.K. Mulleriyawage, W.X. Shen, Impact of demand side management on optimal sizing of residential battery energy storage system, Renewable Energy, Volume 172, 2021, Pages 1250-1266

[10] Barun K. Das, Mahmudul Hasan, Pronob Das, Impact of storage technologies, temporal resolution, and PV tracking on stand-alone hybrid renewable energy for an Australian remote area application, Renewable Energy, Volume 173, 2021, Pages 362-380

[11] Xiaohui Yang, Zhengyang Leng, Shaoping Xu, Chunsheng Yang, Li Yang, Kang Liu, Yaoren Song, Liufang Zhang, Multi-objective optimal scheduling for CCHP microgrids considering peak-load reduction by augmented ε-constraint method, Renewable Energy, Volume 172, 2021, Pages 408-423

[12] Uriel Vargas, George Cristian Lazaroiu, Abner Ramirez, Stability assessment of a stand-alone wind-photovoltaic-battery system via Floquet Theory, Renewable Energy, Volume 171, 2021, Pages 149-158.

[13] A. Emhemed, K. Fong, S. Fletcher and G. Burt, "Validation of Fast and Selective Protection Scheme for an LVDC Distribution Network", IEEE

Transactions on Power Delivery , vol. 32, no. 3, pp. 1432-1440, June 2017.

[14] U. Vargas, G.C. Lazaroiu, E. Tironi and A. Ramirez, “Harmonic Modeling and Simulation of a Stand-alone Photovoltaic- Battery-Supercapacitor Hybrid System”, Elsevier Electrical Power and Energy Systems”, 105 (2019), pp. 70-78.

[15] F. Candeletti, E.Tironi, M. Carminati and E. Ragaini, "LVDC Microgrid with Double AC Grid Interface: Protection Against DC round Faults and Control Strategies". ICHQP, Lubiana 2018

[16] D. Ghaderi, G. Bayrak, J.M. Guerrero, “Grid code compatibility and real-time performance analysis of an efficient inverter topology for PV-based microgrid applications”, *Int. J. of Electrical Power and Energy Systems*, 2021

[17] X. Hu, P. Ma, B. Gao and M. Zhang, "An Integrated Step-Up Inverter Without Transformer and Leakage Current for Grid-Connected Photovoltaic System," in IEEE Transactions on Power Electronics, vol. 34, no. 10, pp. 9814-9827, Oct. 2019.

[18] K.S. Tey, S. Mekhilef, “A reduced leakage current transformerless photovoltaic inverter”, Renewable Energy, Volume 86, 2016, Pages 1103-1112.

[19] J. Jiang, S. Pan, J. Gong, F. Liu, X. Zha and Y. Zhuang, "A Leakage Current Eliminated and Power Oscillation Suppressed Single-Phase Single-Stage Nonisolated Photovoltaic Grid-Tied Inverter and Its Improved Control Strategy," in IEEE Transactions on Power Electronics, vol. 36, no. 6, pp. 6738-6749, June 2021.

[20] M. Carminati, E. Ragaini, S. Grillo and E. Tironi "Currents, Potentials Towords Graund and Fault Protection in DC Microgrids", Proc. AEIT Annual Conference, Trieste, Italy, 18-19 Sept. 2014

[21] M. Carminati, E. Ragaini and E. Tironi, “Overview on Faults and Protections in LVDC Microgrids Connected to the AC Utility”, Int. J. Power Electronics, vol.9, no.3, pp.311-348, 2018.

[22] Z. Shuai, D. He, Z. Xiong, Z. Lei and Z. John Shen, "Comparative Study of Short-Circuit Fault Characteristics for VSC-Based DC Distribution Networks With Different Distributed Generators", IEEE Journal of Emerging and Selected Topics in Power Electronics, vol. 7, no. 1, pp. 528-540, March 2019.

[23] Z. Xiao et al, “An Accurate Analyis Method for Transient Characteristics of DC Line Faults in Voltage Source Converter- Based DC Systems”, IET Generation, Transmission & Distribution, pp. 589-601, 30 November 2020.

[24] Junchao Zheng, Minghao Wen, Yu Chen, Xinan Shao, “A novel differential protection scheme for HVDC transmission lines”, International Journal of Electrical Power & Energy Systems, Volume 94, 2018, Pages 171-178.

[25] Guobing Song, Xu Chu, Xinlei Cai, Shuping Gao, “A novel pilot protection principle for VSC-HVDC cable lines based on fault component current”, International Journal of Electrical Power & Energy Systems, Volume 53, 2013, Pages 426-433.

[26] Xiaodong Zheng, Muhammad Haroon Nadeem, Nengling Tai, Salman Habib, Biqi Wang, Moduo Yu, Yangyang He, “A transient current protection and fault location scheme for MMC-HVDC transmission network”, International Journal of Electrical Power & Energy Systems, Volume 124, 2021, 106348.

[27] J. Yang, J. E. Fletcher and J. O’Reilly, “Multiterminal DC Wind Farm Collection Grid Internal Fault Analysis and Protection Design”, IEEE Trans. on Power Delivery, vol. 25, no 4, pp. 2308-2318, October 2010.

[28] J. Yang, J. E. Fletcher and J. O’Reilly, “Short Circuit and ground Fault Analysis and Location in VSC-Based DC network cables”, IEEE Trans. Ind. Electron., vol.59, pp. 3827-3837, 2012.

[29] D. Bellan, G. Superti-Furga and S.A. Pignari: “Consistent circuit technique for zero-sequence currents evaluation in interconnected single/three-phase power networks”.*Journal of Electrical Systems*, vol. 12, no. 2, June 2016, pp. 230-238.

[30] G. Chicco, P. Postolache, and C. Toader, Analysis of three-phase systems with neutral under distorted and unbalanced conditions in the symmetrical component-based framework, *IEEE Trans. on Power Delivery*, *22*(1), 674-683, 2007.

[31] M. Karimi-Ghartemani, and H. Karimi, Processing of symmetrical components in time-domain, *IEEE Trans. on Power Systems, 22*(2), 572-579, 2007.

[32] D. Bellan, and G. Superti-Furga, “Space-vector state-equation analysis of three-phase transients“. Journal of Electrical Systems, vol. 14, no. 1, March 2018, pp. 188-198

[33] J. M. Aller, A. Bueno, and T. Pagà, “Power system analysis using space-vector transformation,” IEEE Trans. Power Syst., vol. 17, no. 4, pp. 957-965, Nov. 2002.

[34] C. R. Paul, "Decoupling the multiconductor transmission line equations," in IEEE Transactions on Microwave Theory and Techniques, vol. 44, no. 8, pp. 1429-1440, Aug. 1996

[35] C. R. Paul, *Introduction to Electromagnetic Compatibility*, Wiley Interscience, NY: New York, 1992.

[36] Wenjie Chen, Xiaomei Song, Hao Huang and Xu Yang, "Numerical and experimental investigation of parasitic edge capacitance for photovoltaic panel," 2014 International Power Electronics Conference (IPEC-Hiroshima 2014 - ECCE ASIA), Hiroshima, Japan, 2014, pp. 2967-2971.

[37] S. Yu, J. Wang, X. Zhang and F. Li, "Complete parasitic capacitance model of photovoltaic panel considering the rain water," in Chinese Journal of Electrical Engineering, vol. 3, no. 3, pp. 77-84.

[38] ABB White Paper “RC223 (type B) residual-current release”, p.6, October 2009 (https://library.e.abb.com/public/9d3c391e35638d68c1257ac5003ecff9/1SDC007404G0201.pdf)

[39] E.Ragaini, M. Carminati, “A method for detecting ground faults in a LVDC electric line and an electronic device thereof”, EU Patent EP3128335A1 (Feb. 8, 2017).